ADVANCED MATERIALS INTERFACES
www.advmatinterfaces.de

Optical Humidity Sensor Based on CdSe/ZnS Quantum Dots Modified by Porous Silica

*Baozhen Yuan, Xuanyu Zhang, Jiahao Yu, Leiqing Zhou, Bingshen Luo, Yanjun Liu, and Rui Chen**

Ultra-sensitive optical humidity sensors based on nanomaterials play important roles in the fields of science and industry. The related research has been reported, however, the underlying physical mechanism is still unclear. In order to clarify this point, and further improve the sensing performance, herein, optical humidity sensor based on porous silica/quantum dots (PS/QDs) hybrid nanoarchitecture has been developed. PS is selected to enhance emission of QDs due to its large surface roughness, which can improve light utilization. Under optimized conditions, the emission from the hybrid PS/QDs can be enhanced 6.5 times compared with the as-grown QDs. With the increase of relative humidity from 20% to 80%, the hybrid PS/QDs demonstrate excellent response, wide sensing range, fast response time (22–40 s), good selectivity, and repeatability. Based on laser spectroscopy, the sensing mechanism is ascribed to the passivation of the surface defects by water molecules, which results in enhanced emission. This work provides a simple and low-cost method to fabricate humidity sensors and shows promising applications in environmental detection.

1. Introduction

Accurate real-time monitoring and control of ambient humidity are the keys to ensuring high standards in industrial manufacturing, agricultural production, and healthcare,[1–4] as it will severely affect the efficiency and service life of various equipments and systems. An unsuitable relative humidity (RH) environment can significantly affect the performance and stability of optoelectronic devices for energy production, storage, and conversion.[5–7] In addition, humidity can also have unpredictable effects on laboratory experimental results because it changes the physical and chemical properties of nanomaterials.[8] Therefore, the fine control of ambient humidity, especially its useful and rational utilization, is essential for modern and sustainable technologies in different fields. To achieve this, humidity sensors must have high sensitivity, wide humidity detection range, short response and recovery times, as well as excellent durability and reproducibility. However, at present, there are still great challenges to obtain such ideal devices.

Various types of humidity-responsive materials and technologies have been developed over the past few years, such as electrical sensors based on capacitance[9–15] or resistance,[16–18] and optical sensors based on transmission[19] or reflection.[20] All electrical sensors require external power supply which increases the power consumption and integration complexity. Therefore, optical sensors with high performance are emerging. Among various functional materials for optical humidity sensors, semiconductor quantum dots (QDs) may be the most promising materials due to their unique optoelectronic properties, such as size- and composition-tunable photoluminescence (PL) from visible to infrared wavelengths, large absorption coefficient over a broad spectral range and very high levels of brightness and photostability.[21–23] The basic mechanism of QDs-based humidity sensing is to change the PL intensity of QDs by sensing the interactions between water molecules and the QDs surfaces, such as excited state reactions, molecular rearrangements, and energy transfer.[24–26] Generally, special structures are applied to optical humidity sensors for high performance. It has been demonstrated that there are two feasible ways to achieve excellent humidity sensing performance. One is the introduction of the semiconductor-metal heterostructure model. It is well-known that noble metal nanoparticles with localized surface plasmons can significantly enhance light scattering and catalysis, which is beneficial for improving the humidity sensing performance.[27,28] Second, the high surface-to-volume ratio is critical for moisture diffusion and adsorption, which determines the humidity sensitivity, response recovery time, and stability, since the optical properties of QDs are very sensitive to their surface states.[29] Porous silica (PS), as a sol-gel material, is a favorable candidate. PS has been reported to be widely used to immobilize sensitive reagents.[30–34] Compared with surface plasmons, PS possesses the advantages of good biocompatibility, ordered mesoporous structure, large specific surface area, and easy surface modification, which has been widely explored as a proponent of chemical/biosensors, chemical applications, and biochemical reactions and proteomics.[35–38] More importantly, the versatility and convenient

B. Yuan, X. Zhang, J. Yu, L. Zhou, B. Luo, Y. Liu, R. Chen
Department of Electrical and Electronic Engineering
Southern University of Science and Technology
Shenzhen 518055, P. R. China
E-mail: chenr@sustech.edu.cn

The ORCID identification number(s) for the author(s) of this article can be found under https://doi.org/10.1002/admi.202201366.

DOI: 10.1002/admi.202201366

surface chemistry are other attractive advantages, as PS surfaces can achieve any termination required for various wet-chemical functionalization techniques.[39,40]

Recently, sensing devices based on the hybrid of PS and CdTe QDs have hardly been reported and the physical mechanism remains confusing.[41] Therefore, in this work, a humidity sensor with high sensitivity and selectivity based on PS/QDs was developed by dispersing CdSe/ZnS QDs into PS to form a hybrid structure. Morphological and optical property characterizations have been carried out and the experimental results indicate that the sensing film has a good linear response, a wide detection range from 20% to 80% RH, a fast response time of 22 to 40 s, together with good selectivity and recoverability. Finally, the sensing mechanism is verified, which is ascribed to the passivation of PS/QDs surface by water molecules. Our founding provides a simple and low-cost humidity sensor based on PS/QDs, which is important for sensitive environmental detection in the future.

2. Results and Discussion

The absorption and PL spectra of CdSe/ZnS QDs at room temperature are shown in **Figure 1**a. The samples exhibit a relatively broad absorption and a sharp emission peak (λ_{max} = 535 nm) with a small Stokes shift. The inset of Figure 1a shows the transmission electron microscopy (TEM) image of the CdSe/ZnS QDs with uniform size distribution (12 ± 2 nm). The PL spectra of the PS/QDs and as-grown QDs are plotted in Figure 1b. The stable emission peak of PS/QDs implies that PS does not change the energy band structure of QDs. However, PL intensity of PS/QDs enhanced significantly. Figure 1c presents the PL spectra of QDs with different PS ratios. At the beginning, PL intensity increases with the increase of PS and shows a 6.5 times emission enhancement compared to the as-grown QDs when the ratio of PS/QDs is 7. However, due to the nonfluorescent properties, excess PS (the ratio of PS/QDs is over 7) blocks the laser excitation, resulting in a decreased PL intensity. Therefore, the optimal PL enhancement can only be achieved when the proportion of PS is within a moderate range. Scanning electron microscopy (SEM) and TEM images of PS are shown in Figure 1d,e, respectively. The rough surfaces provide favorable conditions for efficient attachment of QDs. Figure 1f exhibits the image of PS/QDs, deducing the uniform attachment of QDs to PS surface, which may be one plausible origin for the enhancement of PL, reducing the emission quenching due to the self-aggregation.[42,43]

Another reason for the enhanced emission may be related to the increased light scattering, which increases the efficiency of light absorption and extraction.[44] It is worth noting that the scattering mentioned herein refers to the multiple scattering events of light that occurs at the numerous QDs/air interfaces due to the rough surface of PS, which leads to an increase in light path length between neighboring particles.[44] In this case, the incident light has more probability to be absorbed by the

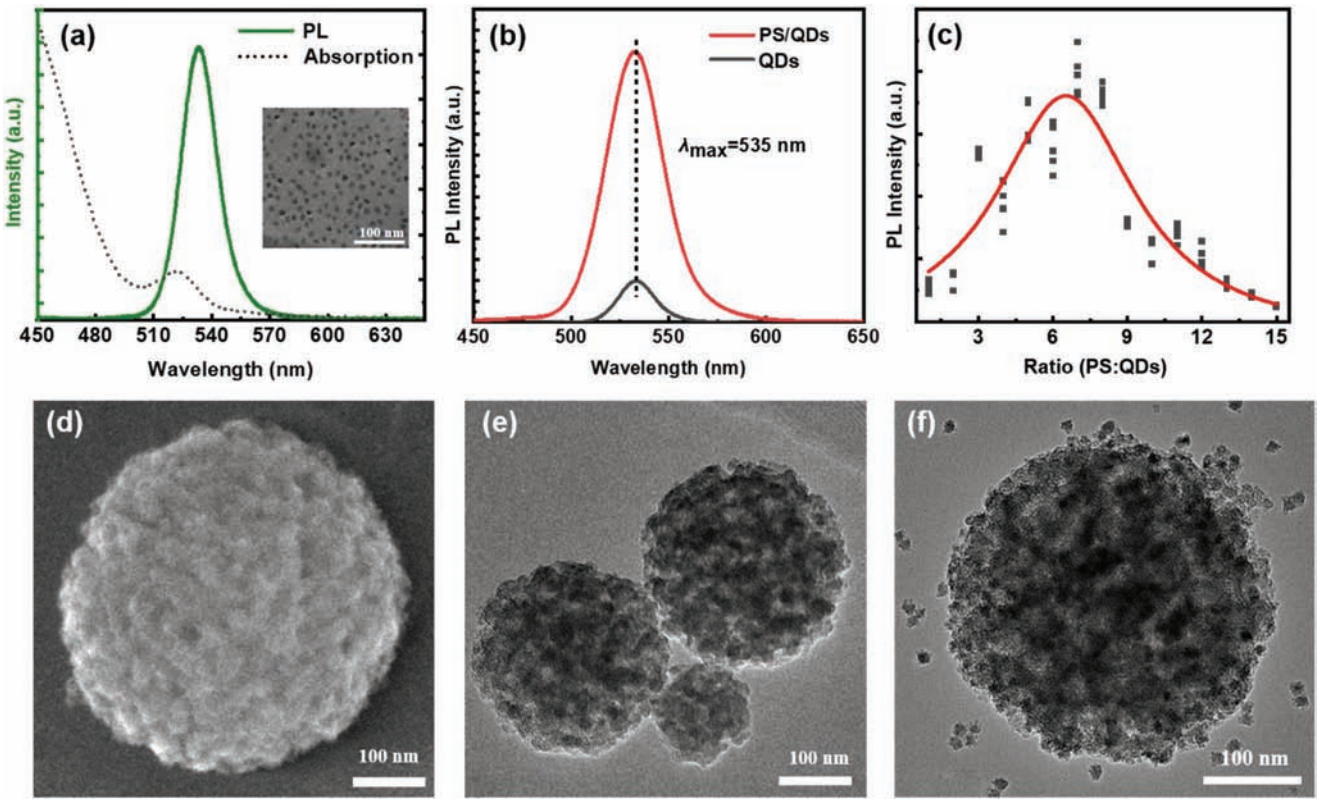

Figure 1. a) Absorption (dash line) and PL (solid line) of CdSe/ZnS QDs at room temperature, respectively. Inset: TEM image of CdSe/ZnS QDs. b) Emission of QDs dispersed in PS. c) PL of QDs dispersed in PS with dif erent ratios. Morphology characterization of PS (d, SEM), (e, TEM) and PS/QDs (f, TEM).

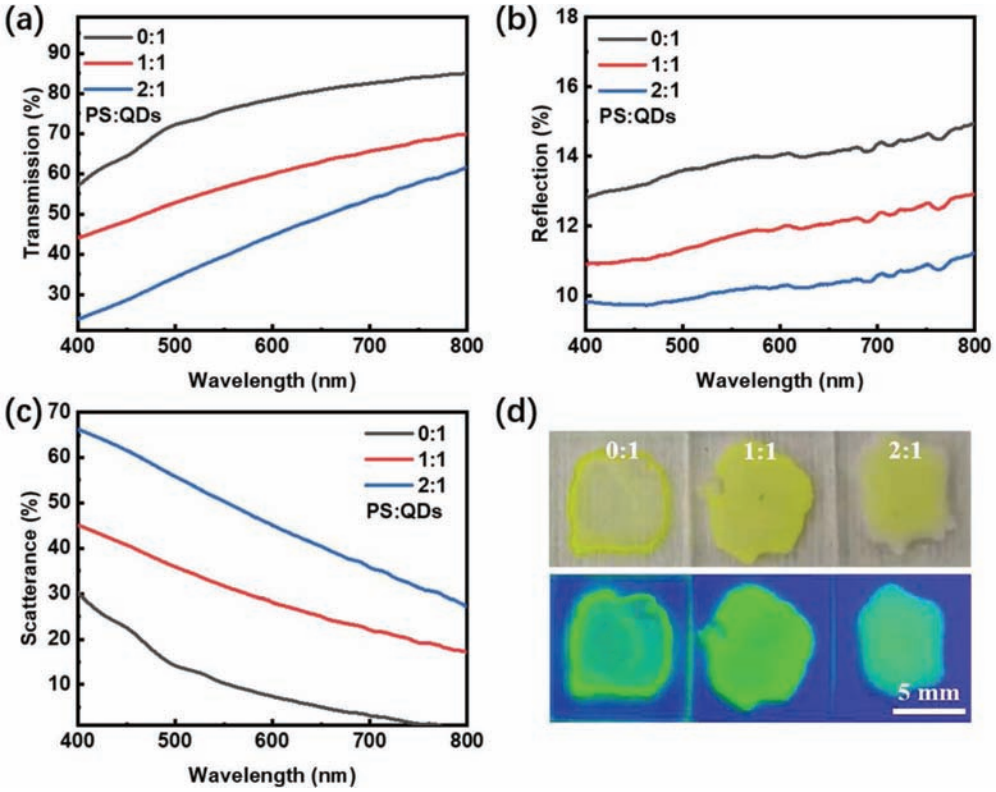

Figure 2. a) Transmission, b) ref ection, and c) scattering of PS/QDs. d) Optical images of the samples with dif erent QD:PS ratios under daylight (above) and UV lamp (below) illumination.

QDs, which in turn enhances the emission. For PS/QDs, the sum of the transmission, reflection, and scattering values of the incident light should be close to 100%, because the absorption of the visible light by silica in PS is negligible. The transmission and reflection measurements of PS/QDs hybrid structures with different ratios (PS:QDs = 0:1, 1:1, 2:1) were carried out to verify the physical mechanism. And the results are shown in **Figure 2**a,b, respectively. The results show that both the transmission and reflection values of PS/QDs decrease with the increase of PS ratio in the range of 400–800 nm. Moreover, the scattering properties of the samples are shown in Figure 2c. It can be seen that the scattering percentage increases with the PS ratio, implying the structure of PS/QDs can increase light scattering, and further enhance the emission. Figure 2d shows the images of the thin films without (top) and with (bottom) UV light illumination. It is noted that PS/QDs have rough surface compared to the as-grown QDs, which is more favorable for scattering. Moreover, PL quantum yields (PLQY), $\lambda_{max,}$ and the full width at half maximum (FWHM) of PS/QDs and the as-grown QDs were measured experimentally, while the data can be seen in **Table 1**. The results show that PLQY of PS/QDs decrease significantly compared to the as-grown QDs, while λ_{max} and FWHM maintain the same. Generally, the value of PLQY will be larger if the QDs are uniformly distributed. Therefore, the results imply that the PL enhancement of PS/QDs is not directed by the reduction of self-aggregation, while the increased light scattering should be responsible for the observation.

Table 1. Emission characteristics of the samples.

Samples	λ_{max} [nm]	PLQY [%]	FWHM [nm]
QDs	529.91	76.90	5.70
PS/QDs	528.42	40.60	5.76

PS/QDs with optimized emission were selected to characterize their humidity sensing characteristics, as shown in **Figure 3**. It can be seen from **Figure 4**a that the PL spectra of the sensing membranes increase linearly with humidity from 20% to 80%. When the humidity is 80%, the PL intensity reaches the maximum value, which is 6.7 times higher than that in 20%. This sensitive response is much higher than another PL-based humidity sensing[41,45] and even comparable to optical-gain-based humidity sensing.[46] This is because the ligands on the surface of QDs are hydrophilic amino groups, which can effectively increase the adsorption of water molecules. The emission response of nanomaterials with RH has been extensively studied, but the mechanism is unclear, as either an increase or decrease of PL intensity with increasing humidity has been observed. Therefore, time-resolved photoluminescence (TRPL) experiment was conducted for verification. It shows that the lifetime of the sensing film at 80% RH is 12.35 ns, which is longer compared to that at 35% RH (9.26 ns), as shown in Figure 4b. It has been reported that this lifetime incensement is the result of a "solvated" surface charged trap state, i.e., the charged trap states are transformed by the adsorbed water molecules with the help of laser irradiation, and eventually, such trap states can be electrostatically inactivated by the adsorbed water molecules.[47–49] After adsorbing of water

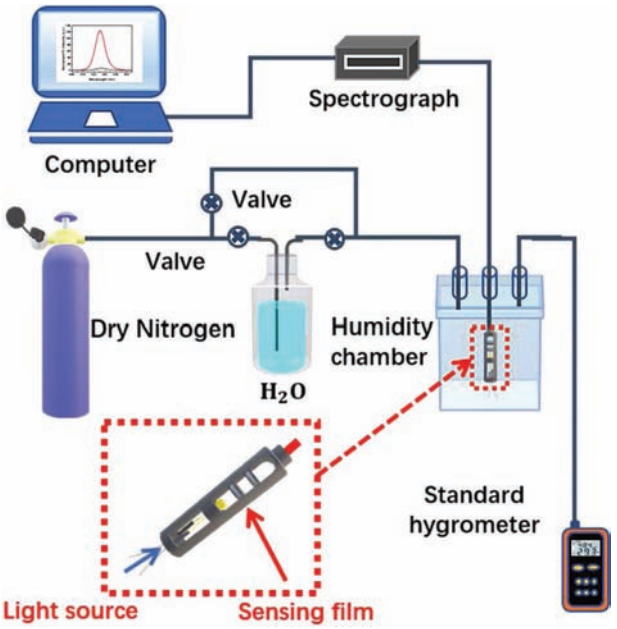

Figure 3. Schematic experimental setup for humidity sensing.

molecules, the PL intensity of PS/QDs increases, especially in high humidity environments, which is consistent with the previous report.[47] In the aerobic environment, two competing processes take place in QDs, that is photo-induced electron transfer of CdSe/ZnS QDs to generate non-emissive QDs and generation of oxygen radical anions, and water stabilization of a highly emissive surface trap state. At high humidity under oxygen, the later one (water stabilization) dominates.

Based on the discussion above, the schematic energy level diagram is proposed to explain the PL enhancement of PS/QDs under high humidity environment, as shown in **Figure 5**a. It is noted that the existence of defect levels leads to a decrease in PL intensity due to non-radiative recombination. With the increase in temperature, bound electrons will escape from defect levels and participate in radiative recombination, and an increase in PL can be observed. Temperature-dependent PL measurements under three different excitation regimes of low (0.02 mW), moderate (0.20 mW), and high (20.0 mW) were conducted to explore the energy position of defects levels, and the PL spectra were presented in Figure S1 (Supporting Information). In Figure 5b, the integrated PL intensity at 60 K was normalized for comparison. It is worth noting that the integrated PL intensity varies greatly with temperature under different excitation conditions. Under low excitation power, the integrated PL intensity shows an unobvious change at low temperature and then increases after the temperature above 260 K. For moderate excitation power, the integrated PL intensity increases more compared to the low excitation power when the temperature exceeds 220 K. Under high excitation power, the integrated PL intensity decreases all the way with temperature. The reason is that at low excitation power, limited number of electrons release from defects levels and compete with the thermal quenching, resulting in enhanced PL. While at moderate excitation power, more electrons are released from the defects levels and contribute to emission, which lead to stronger PL. For high excitation power, the escaped electrons contribute weakly to the emission due to the high density of generated electrons and limited density of defect states, resulting in non-radiative recombination and a decrease in fluorescence intensity with increasing temperature. In addition, laser thermal effects and collisions between electrons can also be more severe. These all lead to the results observed in Figure 5b.

To further discuss the properties of the defects mentioned above, surface treatment was carried out. Normally, surface passivation of organic polymers on semiconductor nanomaterials can effectively reduce the surface defect state density. Since polydimethylsiloxane (PDMS) is a common inert, non-toxic organic polymer material with good optical transparency, it was selected to modify the surface of the sample. PS/QDs were first mixed with PDMS and then dropped on the quartz substrate to prepare the sample, as shown in Figure 5c. Temperature-dependent PL measurements for the as-grown and passivated samples were performed from 60 to 295 K, and the corresponding integrated PL intensity with temperature is shown in Figure 5d. Detailed PL spectra can be found in Figure S2 (Supporting Information). After PDMS treatment, PS/QDs show obvious thermal quenching behavior, which can be ascribed to the reduction of surface defects. Thus, it can be concluded that the defect levels are considered to be the defects located on the surface of the nanomaterials, while the adsorption of water molecules effectively passivates these defects.

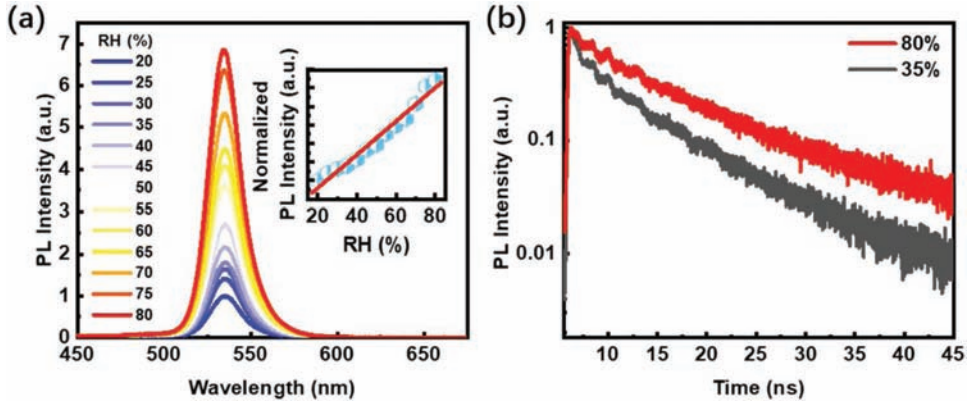

Figure 4. a) Humidity dependent emission of the film. Inset shows the linear dependence of the emission from PS/QDs with humidity. b) PL decay of the emission from the sample under dif erent RH.

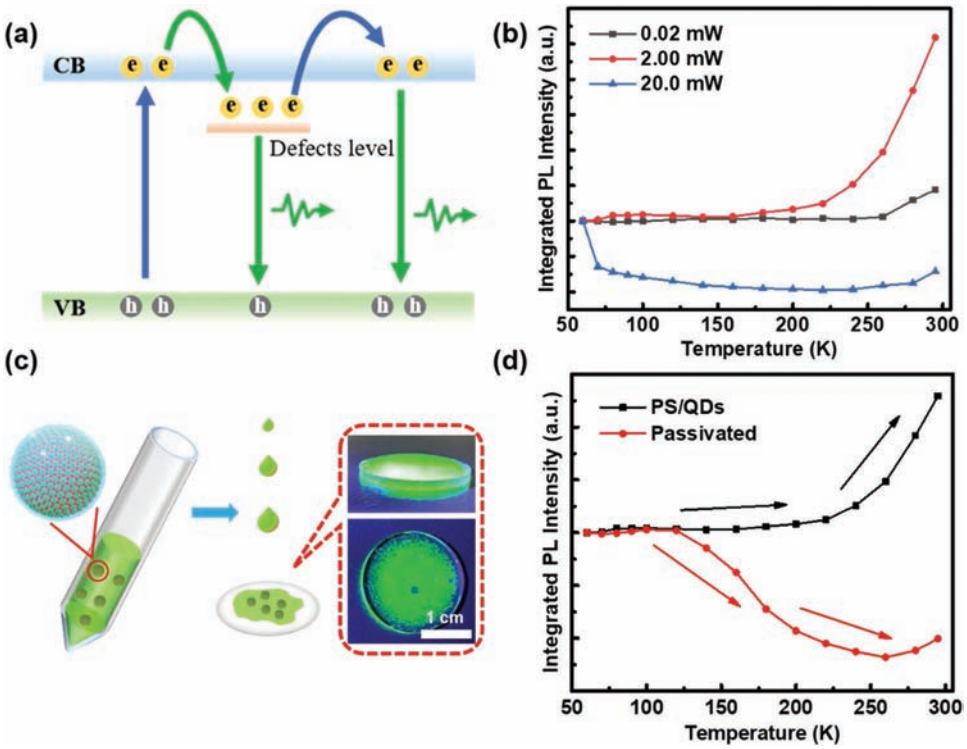

Figure 5. a) The schematic energy diagram of PS/QDs. b) The integrated PL intensity as a function of temperature under dif erent excitation densities. c) Schematic of the passivation of PS/QDs. d) Comparison of the integrated PL intensity as a function of temperature of the film before and after surface passivation.

Finally, the humidity sensing characteristics of the hybrid PS/QDs were discussed. It is known that the response and recovery time are important parameters of sensors. Response time refers to the time from the detector touching the measured humidity to reaching a stable indicated value under test conditions, and the recovery time refers to the time the detector takes for the humidity to return to its initial stable value. **Figure 6**a is the dynamic fluorescence test of the sample under humidity from 40% to 75% at room temperature. It can be seen that the emission intensity of the sample increases gradually with RH and the response time can be determined to be 22 s. Subsequently, when RH decreased from 75% to 40%, the PL intensity decreased and recovered to the initial value, and the response time is 40 s. Besides, other possible interfering gases such as acetone, toluene, ethanol, and *n*-hexane were introduced separately and measured under the same conditions to discuss the selectivity. Particularly, it can be seen from Figure 6b that the PL intensity increased significantly only in the humidity environment. Finally, the reversible characteristics were tested under alternating changes of 30% and 70% RH. As shown in Figure 6c, the PL intensity did not change significantly, which indicates good stability and repeatability. These all demonstrate excellent sensing performances of the humidity sensor based on the PS/QDs studied in this work.

In addition, the comparison of sensing performance from different humidity sensors based on optical signal was summarized

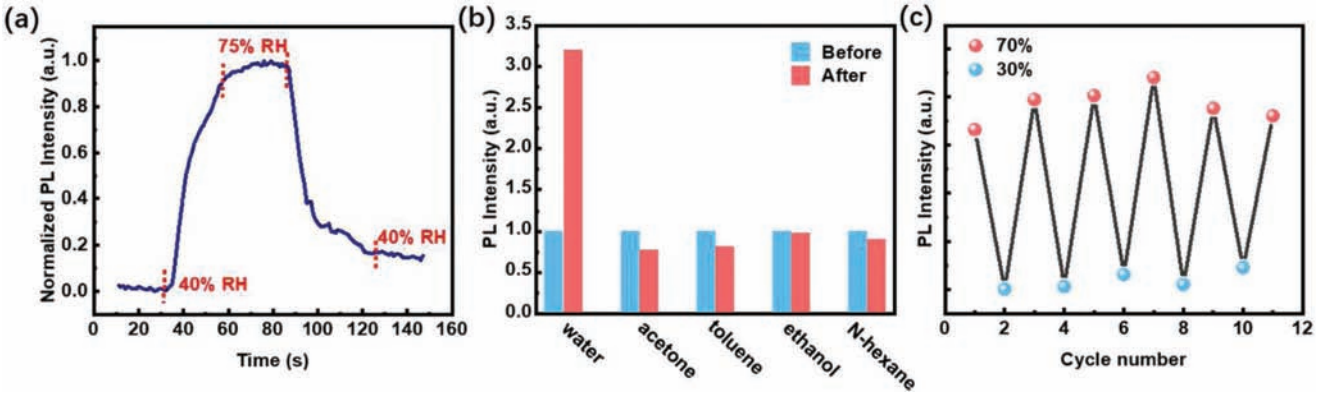

Figure 6. a) Response time, b) selectivity, and c) repeatability of the PS/QDs humidity sensor.

Table 2. Comparison of the sensor performance.

Sensing materials	Detection method	Sensing range [%]	Response time [s]	Ref.
Dye/Polymer	Absorption	0–50	60–90	[50]
CdTe/PS	Fluorescence	12–93	>120	[41]
CdTe@Au/NaOH	Fluorescence	5–97	30	[51]
PVA/QDs-COOH	Fluorescence	10–90	75–240	[45]
Microfiber-Graphene QDs	Peak shifts	0–40	<5	[52]
PS/QDs	Fluorescence	20–80	22	This work

in **Table 2**. Compared with different sensing materials reported so far, the PS/QDs hybrid structure in this work exhibits superior performance, including a wider detection range and a shorter detection time.

3. Conclusion

In summary, a humidity sensor based on hybrid PS/QDs has been successfully developed. Due to the scattering of PS, the PL intensity of PS/QDs is enhanced by a factor of 6.5 times compared with that of the as-grown QDs, which is attractive for sensitive sensing. When PS/QDs film is exposed to RH between 20–80%, the PL intensity increases linearly with humidity and reaches a factor of 6.7 times under 80% RH. Due to the unique surface hydrophilic ligands, this value is much higher than those in other works. Based on laser spectroscopy, it is found that the PL enhancement is due to the effective passivation of surface defects of PS/QDs by water molecules which reduces nonradiative recombination. Thanks to the advanced optical properties of the hybrid PS/QDs, a humidity sensor with a fast response time, good selectivity, and repeatability has been achieved. This simple, low-cost, wide working range humidity sensor not only provides a new convenient way for the design of gas sensor, but also offers a feasible sample for high sensitivity detection based on QDs.

4. Experimental Section

Sample Preparation: Commercially available core-shell CdSe/ZnS QDs coated with amine-derivatized Polyethyleneglycol (PEG-NH_2) (with central emission at 535 nm and diameter of 12 ± 2 nm; 10 nmol L^{-1}) was purchased from Xingshuo Nanotech Co., Ltd. (Jiangsu, China). PS particles with an average size of 400–900 nm and a specific surface area of 2 m^2 g^{-1} were purchased from XFNANO (Jiangsu, China). PS/QDs hybrid structure was fabricated by dispersing QDs into PS. The CdSe/ZnS QDs and PS/QDs were respectively drop-casted on the surface of a quartz plate to fabricate solid films used for lateral optical measurements. PDMS (Sylgard 184 Silicon, Dow Corning) was prepared by mixing liquid silicon matrix base and curing agent with a mass ratio of 10:1. Then, the colloidal PDMS was well mixed with PS/QDs and dropped on the film. Finally, PDMS was cured by heating at 60 °C for 30 min. The lower curing temperature ensures that the PS/QDs are not damaged during the process.

Optical Characterization: The absorption measurements were performed by a Lambda 950 UV–vis spectrophotometer (PerkinElmer). For PL measurement, all samples were excited by a 325 nm He-Cd laser (KIMMON IK5751I-G), and the signal was detected by a Newton CCD (DU920P-BU) integrated with Shamrock monochromator (SR-750-D1-R). The ref ection and transmission of the PS/QDs film were measured by a UV-Vis-NIR microspectrophotometer (CRAIC technologies Inc.) with a xenon lamp used as the illumination source. Absolute PLQY measurements were performed by a spectrometer (Zolix, SENS-9000). TRPL experiments were carried out at room temperature. The excitation source was a pulsed ultraviolet picosecond diode laser operating at 375 nm. The pulse width and repetition rate of the laser were 40 ps and 20 MHz, respectively. The signal was dispersed by a 320 mm monochromator (iHR320 from Horiba, Ltd.) combined with suitable filters and detected based on the time-correlated single photon counting technique. For the temperature-dependent PL measurements, the sample was placed inside a closed-cycle helium cryostat with quartz windows (CRYO Cool-G2B-LT). The temperature during PL measurement was well-controlled from 60 to 295 K.

Morphology Characterization: SEM (Hitachi S-4800) was used to measure the microstructures of PS. TEM (FEI Talos F200X) operated at 200 kV was used to characterize the size and shape of the CdSe/ZnS QDs, PS, and PS/QDs, respectively.

Humidity Characterization: The humidity was adjusted according to the ratio of nitrogen and water in the chamber with precise control of gas f ow. At the beginning, the valve on the upper end of the gas collecting cylinder was opened, and the gas in the chamber was exhausted by introducing nitrogen gas, so as to avoid the contact between the QDs and air. After the air was exhausted, this valve was closed and the valves at the left and right ends of the gas collecting cylinder were opened, and then used nitrogen to volatilize water vapor into the chamber. The amount of water vapor entering the chamber determined the humidity in the chamber. To reduce humidity, the valves at both ends of the gas collecting cylinder were closed, the upper valve was opened and dry nitrogen f owed into the chamber. Therefore, humidity could be controlled by repeatedly changing the valves. Besides the humidity cavity, there are important parts of the sensor including the sensing material, standard hygrometer, and spectrometer. The excitation light source used during the experiment is a He-Cd laser (λ = 325 nm) and all test gases are in an air-isolated condition to avoid the inf uence of the external environment.

Supporting Information

Supporting Information is available from the Wiley Online Library or from the author.

Acknowledgements

B.Z.Y. and X.Y.Z. contributed equally to this work. This work is supported by National Natural Science Foundation of China (62174079), Science, Technology and Innovation Commission of Shenzhen Municipality (Projects Nos. JCYJ20210324120204011 and KQTD2015071710313656), Special Funds for the Cultivation of Guangdong College Students' Scientific and Technological Innovation (pdjh2021c0019).

Conf ict of Interest

The authors declare no conf ict of interest.

Data Availability Statement

The data that support the findings of this study are available from the corresponding author upon reasonable request.

Keywords

CdSe/ZnS quantum dots, humidity sensing, porous silica, scattering, surface defects

Received: June 18, 2022
Revised: July 25, 2022
Published online: September 7, 2022

[1] L. Chao, C. Hu, J. Luo, S. Liu, Y. Qiao, Z. Zhang, J. Song, Y. Shi, J. Cai, A. Watanabe, *Nanomaterials* **2019**, *9*, 422.
[2] T. Li, L. Li, H. Sun, Y. Xu, X. Wang, H. Luo, Z. Liu, T. Zhang, *Adv. Sci.* **2017**, 4, 1600404.
[3] Y.-T. Jao, P.-K. Yang, C.-M. Chiu, Y.-J. Lin, S.-W. Chen, D. Choi, Z.-H. Lin, *Nano Energy* **2018**, 50, 513.
[4] W. Jeong, J. Song, J. Bae, K. R. Nandanapalli, S. Lee, *ACS Appl. Mater. Interfaces* **2019**, 11, 44758.
[5] D. Li, E.-J. Borkent, R. Nortrup, H. Moon, H. Katz, Z. Bao, *Appl. Phys. Lett.* **2005**, 86, 042105.
[6] C. Chen, T. F. Fuller, *Polym. Degrad. Stab.* **2009**, *94*, 1436.
[7] N. Grossiord, J. M. Kroon, R. Andriessen, P. W. M. Blom, *Org. Electron.* **2012**, 13, 432.
[8] P. Fotios, K. M. Papazisi, T. Dintzer, V. Papaefthimiou, V. A. Saveleva, S. P. Balomenou, D. Tsiplakides, F. Bournel, J. Gallet, S. Zafeiratos, *ACS Appl. Mater. Interfaces* **2017**, *9*, 25265.
[9] J.-G. Liang, C. Wang, Z. Yao, M.-Q. Liu, H.-K. Kim, J. M. Oh, N.-Y. Kim, *ACS Appl. Mater. Interfaces* **2018**, 10, 851.
[10] X. Zhao, Y. Long, T. Yang, J. Li, H. Zhu, *ACS Appl. Mater. Interfaces* **2017**, *9*, 30171.
[11] D. Wang, D. Zhang, P. Li, Z. Yang, Q. Mi, L. Yu, *Nano-Micro Lett.* **2021**, 13, 57.
[12] D. Zhang, Z. Xu, Z. Yang, X. Song, *Nano Energy* **2020**, 67, 104251.
[13] X. Liu, D. Zhang, D. Wang, T. Li, X. Song, Z. Kang, *J. Mater. Chem. A* **2021**, *9*, 14524.
[14] D. Zhang, D. Wang, P. Li, X. Zhou, X. Zong, G. Dong, *Sens. Actuators, B* **2018**, 255, 1869.
[15] D. Wang, D. Zhang, Y. Yang, Q. Mi, J. Zhang, L. Yu, *ACS Nano* **2021**, 15, 2911.
[16] S. Wang, Z. Chen, A. Umar, Y. Wang, T. Tian, Y. Shang, Y. Fan, Q. Qi, D. Xu, *J. Phys. Chem. C* **2015**, 119, 28640.
[17] K. Jiang, H. Zhao, J. Dai, D. Kuang, T. Fei, T. Zhang, *ACS Appl. Mater. Interfaces* **2016**, 8, 25529.
[18] H. Guo, J. Chen, L. Tian, Q. Leng, Y. Xi, C. Hu, *ACS Appl. Mater. Interfaces* **2014**, 6, 17184.
[19] E. Tian, J. Wang, Y. Zheng, Y. Song, L. Jiang, D. Zhu, *J. Mater. Chem.* **2008**, 18, 1116.
[20] Y. J. Liu, J. Shi, F. Zhang, H. Liang, J. Xu, A. Lakhtakia, S. J. Fonash, T. J. Huang, *Sens. Actuators, B* **2011**, 156, 593.
[21] S. M. Ng, M. Koneswaran, R. Narayanaswamy, *RSC Adv.* **2016**, 6, 21624.
[22] C. J. Murphy, *Anal. Chem.* **2002**, 74, 520A.
[23] K. Zhang, H. Zhou, Q. Mei, S. Wang, G. Guan, R. Liu, J. Zhang, Z. Zhang, *J. Am. Chem. Soc.* **2011**, 133, 8424.
[24] A. Hässelbarth, A. Eychmüller, H. Weller, *Chem. Phys. Lett.* **1993**, 203, 271.
[25] Z. Liang, M. Kang, G. F. Payne, X. Wang, R. Sun, *ACS Appl. Mater. Interfaces* **2016**, 8, 17478.
[26] Y. Li, H. Sun, F. Shi, N. Cai, L. Lu, X. Su, *Biosens. Bioelectron.* **2015**, 74, 284.
[27] S. M. Majhi, P. Rai, S. Raj, B.-S. Chon, K.-K. Park, Y.-T. Yu, *ACS Appl. Mater. Interfaces* **2014**, 6, 7491.
[28] S. K. Das, E. Marsili, **2011**: Croacia: InTech.
[29] H. Xia, J. Hu, J. Tang, K. Xu, X. Hou, P. Wu, *Sci. Rep.* **2016**, 6, 36794.
[30] C. McDonagh, C. S. Burke, B. D. MacCraith, *Chem. Rev.* **2008**, 108, 400.
[31] P. C. Jerónimo, A. N. Araújo, M. C. B. Montenegro, *Talanta* **2007**, 72, 13.
[32] G. Orellana, D. Haigh, *Curr. Anal. Chem.* **2008**, 4, 273.
[33] A. Lukowiak, W. Strek, *J. Sol-Gel Sci. Technol.* **2009**, 50, 201.
[34] M. Liu, T. Li, C. Zhang, Y. Zheng, C. Wu, J. Zhang, K. Zhang, Z. Zhang, *J. Hazard. Mater.* **2021**, 415, 125699.
[35] M. Hartmann, X. Kostrov, *Chem. Soc. Rev.* **2013**, 42, 6277.
[36] Q. Lei, J. Guo, A. Noureddine, A. Wang, S. Wuttke, C. J. Brinker, W. Zhu, *Adv. Funct. Mater.* **2020**, 30, 1909539.
[37] A. Y. Fadeev, V. A. Eroshenko, *J. Colloid Interface Sci.* **1997**, 187, 275.
[38] B. Lee, Y. Kim, H. Lee, J. Yi, *Microporous Mesoporous Mater.* **2001**, 50, 77.
[39] Z. Shen, J. J. Thomas, C. Averbuj, K. M. Broo, M. Engelhard, J. E. Crowell, M. G. Finn, G. Siuzdak, *Anal. Chem.* **2001**, 73, 612.
[40] A. Erigoni, U. Diaz, *Catalysts* **2021**, 11, 79.
[41] J. Hu, P. Wu, D. Deng, X. Jiang, X. Hou, Y. Lv, *Microchem. J.* **2013**, 108, 100.
[42] H. C. Kim, H.-G. Hong, C. Yoon, H. Choi, I.-S. Ahn, D. C. Lee, Y.-J. Kim, K. Lee, *J.Colloid Interface Sci.* **2013**, 393, 74.
[43] K. Um, H.-J. Kim, J. H. Jo, H. Jeon, H.-B. Yang, Y.-J. Kim, K. Lee, *Chem. Eng. J.* **2019**, 369, 109.
[44] J. Ryu, J. Yun, J. Lee, K. Lee, J. Jang, *Chem. Commun.* **2016**, 52, 2165.
[45] Y. Cheng, H. Wang, L. Li, T. Han, X. Liang, L. Dong, *Sens. Actuators, B* **2019**, 284, 258.
[46] W. Chen, X. Lu, F. Fan, J. Du, *Nano Lett.* **2021**, 21, 7732.
[47] K. Pechstedt, T. Whittle, J. Baumberg, T. Melvin, *J. Phys. Chem. C* **2010**, 114, 12069.
[48] M. Oda, A. Hasegawa, N. Iwami, K. Nishiura, N. Ando, A. Nishiyama, H. Horiuchi, T. Tani, *J. Lumin.* **2007**, 127, 198.
[49] C. Meng, Y. Xiao, P. Wang, L. Zhang, Y. Liu, L. Tong, *Adv. Mater.* **2011**, 23, 3770.
[50] M. D. Fernández-Ramos, Y. F. Ordóñez, L. F. Capitán-Vallvey, I. M. P. de Vargas-Sansalvador, J. Ballesta-Claver, *Sens. Actuators, B* **2015**, 220, 528.
[51] M. Chen, S. Xue, L. Liu, Z. Li, H. Wang, C. Tan, J. Yang, X. Hu, X.-F. Jiang, Y. Cheng, H. Wang, X. Xing, S. He, *Sens. Actuators, B* **2019**, 287, 329.
[52] V. Ruiz, I. Fernández, P. Carrasco, G. Cabañero, H. J. Grande, J. Herrán, *Sens. Actuators, B* **2015**, 218, 73.